Monitoring the failure mechanisms of a reinforced concrete beam strengthened by textile reinforced cement using acoustic emission and digital image correlation

Dimitrios G. Aggelis[*], Svetlana Verbruggen[a], Eleni Tsangouri[b], Tine Tysmans[c] and Danny Van Hemelrijck[d]

Department of Mechanics of Materials and Constructions, Vrije Universiteit Brussel, Pleinlaan 2, 1050 Brussels, Belgium

Abstract. One of the most commonly used techniques to strengthen steel reinforced concrete structures is the application of externally bonded patches in the form of carbon fiber reinforced polymers (CFRP) or recently, textile reinforced cements (TRC). These external patches undertake the tensile stress of bending constraining concrete cracking. Development of full-field inspection methodologies for fracture monitoring are important since the reinforcing layers are not transparent, hindering visual observation of the material condition underneath. In the present study acoustic emission (AE) and digital image correlation (DIC) are applied during four-point bending tests of large beams to follow the damage accumulation. AE helps to determine the onset of fracture as well as the different damage mechanisms through the registered shifts in AE rate, location of active sources and change in waveform parameters. The effect of wave propagation distance, which in large components and in-situ can well mask the original information as emitted by the fracture incidents is also discussed. Simultaneously, crucial information is supplied by DIC concerning the moments of stress release of the patches due to debonding, benchmarking the trends monitored by AE. From the point of view of mechanics, conclusions on the reinforcing contribution of the different repair methodologies are also drawn.

Keywords: acoustic emission; digital image correlation; cracking; debonding; externally bonded reinforcement; frequency; RA value

1. Introduction

Classification of acoustic emission (AE) signals emitted during discrete failure processes enables the assessment of the condition of a concrete structure. The reason is the sequence of different fracture modes initiating with concrete cracking at lower loads leading to

---

*Corresponding author, Professor, E-mail: daggelis@vub.ac.be
[a] Post-doc researcher, E-mail: Svetlana.verbruggen@vub.ac.be
[b] Post-doc researcher, E-mail: Eleni.tsangouri@vub.ac.be
[c] Professor, E-mail: tine.tysmans@vub.ac.be
[d] Professor, E-mail: danny.van.Hemelrijck@vub.ac.be

shear/debonding failures approaching the ultimate failure load (Ohtsu 2010, Ohno and Ohtsu 2010, Shahidan *et al.* 2013). Therefore, reliable characterization of the AE sources, may provide a warning before failure reaches its final stage. The technique of AE utilizes sensors mounted on the surface of the material receiving the elastic waves emitted by the motion of the crack tips and transforming them into waveforms through their piezoelectric element (Grosse and Ohtsu 2008). Some of the most important waveform characteristics are the maximum voltage (amplitude, A in dB), the number of threshold crossings (counts) and the duration (time between the first and last threshold crossings in µs). The rise time (RT in µs) is the time between the first threshold crossing and the waveform peak amplitude, see Fig. 1, while the threshold is defined by the user in order to avoid ambient noise. A frequency feature is the average frequency (AF in kHz), which is the number of counts over the duration, while the central frequency, CF (centroid of the FFT spectrum in kHz) is also used. Additionally, the "RA" value is the ratio of RT over A and is measured in µs/V. The number of recorded signals (hits) yields information on the active fracturing points and contributes to the monitoring of processes like fracture (Carpinteri *et al.* 2008, Karihaloo *et al.* 2013), creep (Verstrynge *et al.* 2009), corrosion (Uddin *et al.* 2006) and self-healing (Van Tittelboom *et al.* 2012). Localization of the sources is also possible in three dimensions if multiple sensors are applied (Luo *et al.* 2006, Ge 2003). In order to obtain qualitative information on the damage mode several waveform shape parameters have been examined. Recently it has been shown that frequency values decrease for shear cracking compared to tensile failure. Additionally, RT and RA increase substantially due to the higher proportion of shear waves that are emitted by shear cracks (Aggelis 2011). These trends have been exploited in laboratory conditions with satisfactory characterization of the AE sources (Ohtsu 2010, Aggelis 2011, Shahidan *et al.* 2013, Farhidzadeh *et al.* 2013). The classification is based on the AF-RA axes in which the tensile and shear cracking data exhibit very limited overlap in numerous laboratory cases so that they can be separated even by a single line.

In this paper, the results of AE monitoring on externally reinforced large scale concrete beams are presented. Three beam types are compared in a four point bending test: a reference beam, a beam with a Textile Reinforced Cementitious composite (TRC) as external reinforcement and a beam externally reinforced with a CFRP strip. The TRC consists of an Inorganic Phosphate Cement (IPC) matrix strengthened with 2D random glass fiber textiles. The focus in this paper is on the behavior of the TRC reinforced beam.
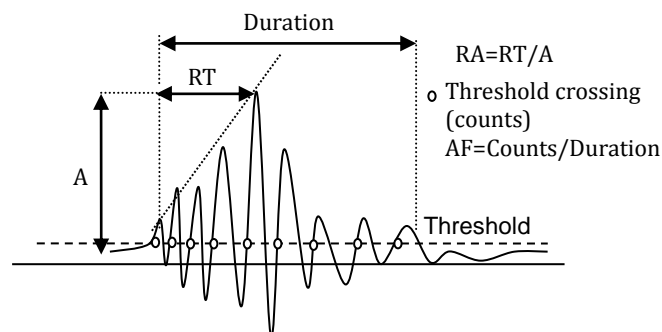

Fig. 1 Typical AE signal and its main characteristics

The importance of this study lies in both the mechanical behavior and the monitoring methodology. First the mechanical performance of the different reinforcing methods is discussed and compared to the reference beam. More importantly, since the external layers usually do not allow direct observation as they are not transparent, passive monitoring techniques are used in order to build experience in evaluating the condition in a passive nonintrusive way. Apart from AE, the monitoring is accompanied by digital image correlation (DIC) in order to confirm the trends in crucial loading moments. DIC is a non-contact optical technique, capable of measuring and calculating surface displacements and strains by the comparison of subsequent pictures taken with 2 CCD cameras facing a speckle pattern applied on the specimen's surface (Sutton *et al.* 2009). The combination of the DIC strain fields with the AE signals analysis benchmarks the results concerning failure. Discussion is also done about the application of AE classification in large scale since the stress waves are attenuated and scattered by the heterogeneous texture of concrete including aggregates, metallic reinforcing bars, voids and cracks.

2. Experimental details

2.1 Materials and mechanical testing

Four-point bending tests were performed on the three beam types with a total length of 2.5 m (middle span length of 2.3 m) and height and width of 0.3 m and 0.2 m respectively (Fig. 2). The loading was displacement controlled by a servo-hydraulic actuator with an initial displacement rate of 0.2 mm/min, increasing to 2 mm/min after the load of 60 kN.

The beams were cast with concrete of 35.0 MPa compressive strength, Young modulus of 34.0 GPa and a modulus of rupture of 5.3 MPa after 48 days. The internal steel reinforcement (S500) consisted of two longitudinal bars with a diameter of 16 mm and stirrups with a diameter of 6 mm placed every 100 mm across the shear zones of the beams (Fig. 2). This shear reinforcement is overdimensioned in order to achieve beam failure in bending, as both AE and DIC focus on the central zone of constant bending moment.

The external TRC reinforcement covered the full bottom surface of the beam. It consisted of an IPC matrix reinforced with 16 randomly in-plane oriented fibre textiles, being chopped strand mats Vetrotex M5, with a surface density of 300 g/m², resulting in a fibre volume fraction of 21%. These laminates have a tensile strength of 58.4 MPa, an ultimate strain of 1.2%, a Young modulus at the un-cracked stage of 12.5 GPa and at the fully cracked stage of 4.8 GPa.

The CFRP strip (TRADECC 2007) had a standard thickness of 1.2 mm and a width of 30 mm, so as to obtain the same ultimate load as the TRC reinforced beam, following the FIB bulletin 14 (CEB-FIB 2001). The CFRP strip, had a tensile strength of 2.21 GPa and a Young's modulus of 143 GPa. In all cases the external reinforcement was glued onto the concrete using a two-component epoxy glue (PC 5800/BL (TRADECC 2009)). Before attaching the reinforcement to the beams, the concrete surface was pretreated to remove the laitance layer. It is mentioned that although CFRP exhibit higher tensile strength, their performance is compromised by temperature. In order to improve the tensile behavior of TRC a large content of fibres is used, enabled by the fine microstructure of the material (grain size less than 100 μm). More specific information on the material and its development can be found in literature (Täljsten *et al.* 2007, Ombres 2011, European Patent Office 2000, Verbruggen *et al.* 2012, Verbruggen 2014).
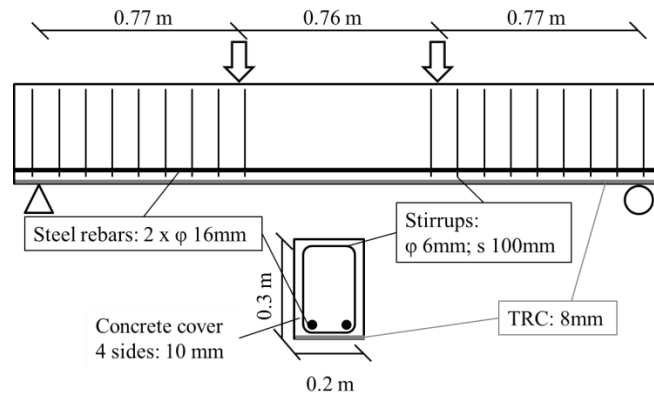
Fig. 2 Test set-up and reinforcement scheme

2.2 Acoustic emission

In total eight AE sensors were applied at the center of the beams. Five sensors were placed at one side, (see Fig. 3) and three at the top while the other two sides were covered by the DIC speckle pattern. Three sensors were of the WD (PAC) type with broadband response and center at 500 kHz and five were R15 (PAC) with resonance of 150 kHz. The sensors covered the central part of the beams, spreading 150 mm at either side of the center (maximum horizontal separation distance on a surface 300 mm, while the lowest two sensors were placed 50 mm above the bottom. The wideband sensors were placed at higher elevations (200 mm), while the resonant sensors were attached close to the bottom in order to capture the activity even from the small scale cracking. The threshold was set at 35 dB and the acquired signals were pre-amplified and stored in a PAC micro-II 8 channel system. While for location purposes all eight sensors were used, for the parameter analysis in this paper the discussion is restricted to the broadband sensors in order to have a broader range of frequency values.
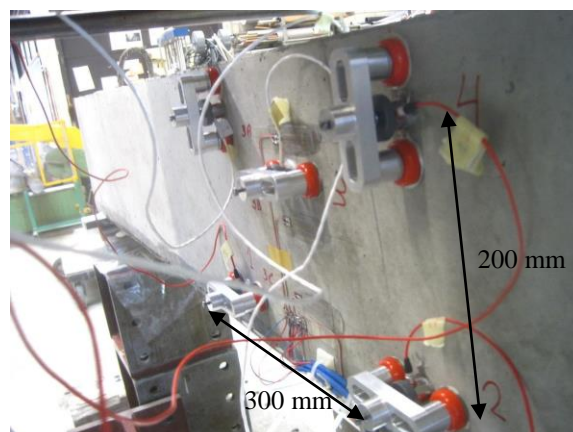

Fig. 3 A snapshot during testing of the TRC reinforced beam with AE sensors. Magnetic clamping devices are applied to support the sensors
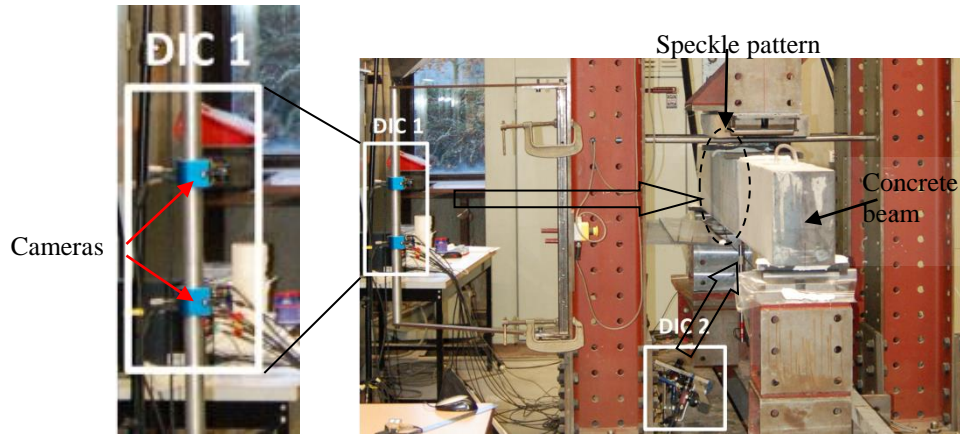
Fig. 4 Schematic overview of the 2 DIC systems used

3. Digital image correlation

Two DIC systems were used to monitor the deformation at the constant moment zone of the beams (central zone with a width slightly larger than 0.4 m). One pair of DIC cameras visualized one vertical side of the beam (DIC 1 in Fig. 4) and the second one the bottom side (DIC 2 in Fig. 4). The number of pixels was 2452 x 2056. This results in a magnification factor of 0.1876 mm/px. A theoretical accuracy of the displacement corresponds to 0.01 px (Sutton *et al.* 2009) and thus the smallest theoretical measurable displacement is 1.9 µm. Comparison of two images at zero load results in a strain variation between -0.046% and 0.046%, which is the noise level. Pictures were captured every 0.2 kN and every 5 seconds. The correlation analysis was done using the VIC3D-2009 software package from Correlated Solutions where a subset size of 21 pixels, a step size of 5 pixels and a strain window size of 11 were chosen.

4. Results

4.1 Mechanical performance

Concerning the mechanical performance, the TRC reinforced beam exhibited a 37% higher maximum load compared to the reference (210 kN over 153 kN). The CFRP reinforced beam reached 190 kN being in between. The externally reinforced beams displayed some instantaneous load drops before reaching their maximum bending capacity which are results of partial delaminations of the CFRP strip and the TRC layer, see Fig. 5. In this study the AE behaviour during the load drops of the TRC beam (see arrows in Fig. 5) are of particular importance and are analyzed at the following sections, while a previous study focused on the CFRP (Aggelis *et al.* 2013).

4.2 Total AE activity and fracture mode

The overall AE activity of the beams is shown in Fig. 6. The reference and the CFRP reinforced beam started registering events at load levels below 20 kN, while the TRC-reinforced started to register events at the load of 40 kN, indicating the effective delay of the cracking onset. Additionally, for any load the TRC beam emitted a lower amount of AE signals than any of the other two beams. Indicatively, at the load of 100 kN, the TRC reinforced beam had recorded 211 events, the CFRP reinforced 302 events while the reference beam 585 events, showing that a much more severe damage was accumulated. After the maximum load, in most cases large cracks were developed, resulting in detachment of some of the sensors and ending therefore, the possibility to record more events.
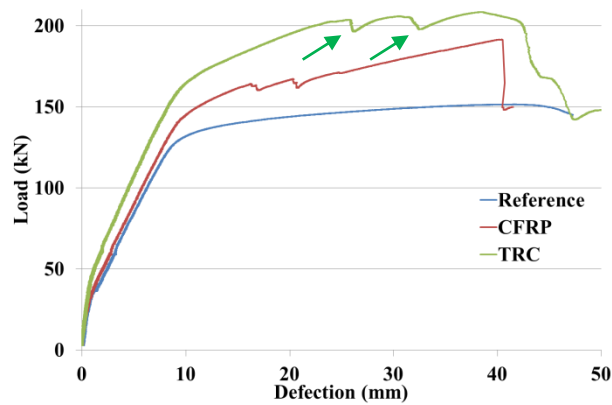

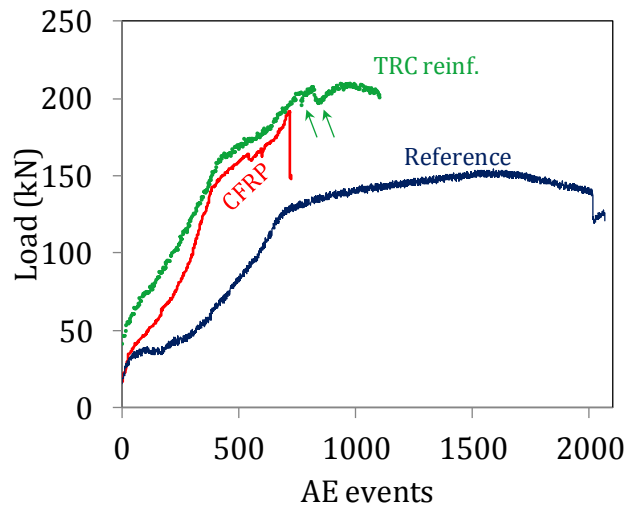Fig. 5 Load vs. deflection curves for the different beams

Fig. 6 Load vs. AE activity for different beams

Additional to the cumulative AE activity it is worth studying specific waveform parameters that reveal information on the fracture mode of the sources. On that direction, the discrimination between the concrete cracking events and debonding of the external reinforcing layer exhibits particular interest. The reason is the lack of visual contact that does not permit the detection of the damage developed beneath the reinforcing patch/layer. In order to study this, the AE activity during debonding moments of the TRC layer was isolated and compared to indicative populations of concrete cracking events. The "debonding" signals were selected based on their acquisition time, since they were received during the moments of load drop, shown by the arrows in Figs. 5 and 6. The activity at these short time windows (less than 1 s each) was isolated using the Noesis software, adding up to 449 hits. The majority of the AE events were located within 50 mm from the bottom of the beam while at these moments DIC revealed a strain release in the TRC layer, as will be shown later, which provided a profound indication of debonding. The characteristics of these hits are compared with an indicative population of AE signals that occurred as the load was monotonically increasing (just before, after and in between the two load drops) adding up to 2000 hits.

Table 1 shows the average values of AE waveform parameters for concrete cracking as well as for TRC debonding moments. A typical debonding signal has longer duration and rise time and higher RA value, while the cracking hits are characterized by higher frequency content in the form of the average or CF. These enlightening results indicate that the different fracture mechanisms can potentially be characterized even in large scale structures, despite the strong overlap between the characteristics of the various sources. Fig. 7(a) depicts the correlation between AF and AE duration. The two populations are overlapping in large part of the plot but the averages can be distinguished, especially in terms of duration. Fig. 7(b) shows the plot of AF vs. RA values, a commonly applied correlation for classification purposes (Ohtsu 2010, Aggelis 2011). In this case the overlap seems stronger, although the averages are again far apart. This overlap is mainly attributed to two reasons. One is the random nature of concrete fracture. Each fracture event cannot be identical to the previous and therefore, any variability is inevitably transferred to the AE events. Another reason for the experimental scatter is the varying distance between the AE sources and the sensors. The elastic waves undergo strong attenuation and distortion due to the inhomogeneity of the medium (Aggelis *et al*. 2012). The distortion depends on the length of the propagation path. The sensors that are located close to a source receive a waveform closer to the emitted one, while others that stand further (centimeters up to meters) receive a strongly distorted waveform. These phenomena make classification of AE events troublesome in real structures as they cause a high error factor, masking the original information of the crack tip movement.

4.3 Effect of wave propagation on AE

Reinforced concrete members are heterogeneous systems due to porosity, cavities, aggregates and metal reinforcement. Elastic waves are bound to undergo damping and scattering altering the waveform characteristics with eventual consequences in the accuracy of characterization. To demonstrate the effect of propagation dependency of the AE signals, Fig. 8(a) shows the average RA for different classes of AE signals, relative to the delay time to the sensors. The AE hits of the classified events were divided in three groups according to their acquisition delay to the sensor; 0-50 μs, 50-100 μs and greater than 100 μs. Due to the decreasing amplitude and the stretching of the waveforms in time due to scattering, the RA rises for longer distances, as already numerically investigated (Aggelis *et al*. 2012). In the case of sources recorded by sensors within 50 μs delay

(or approximately in the range of 200 mm considering a wave velocity of 4000 m/s) concrete cracking is characterized by RA of approximately 3.8 ms/V, and debonding by 5.5 ms/V. However, due to distortion effect, concrete cracking signals that propagated an additional distance of 200 mm (or 50 µs more) exhibited an average RA of 6 ms/V, and can be easily mistaken for debonding events that propagated shorter. AE hits that propagated even longer (delay more than 100 µs) had an average value above 8 ms/V. Similar effect is observed in the case of energy analysis, but with inverse trend. Fig. 8(b) shows the energy trend of the AE signals (measured area under the rectified signal envelope, MARSE) over the additional delay time after reception at the first sensor. In this particular case, concrete cracking signals carry a larger amount of energy (more than 20%) compared to the debonding ones for the same propagation distance range.
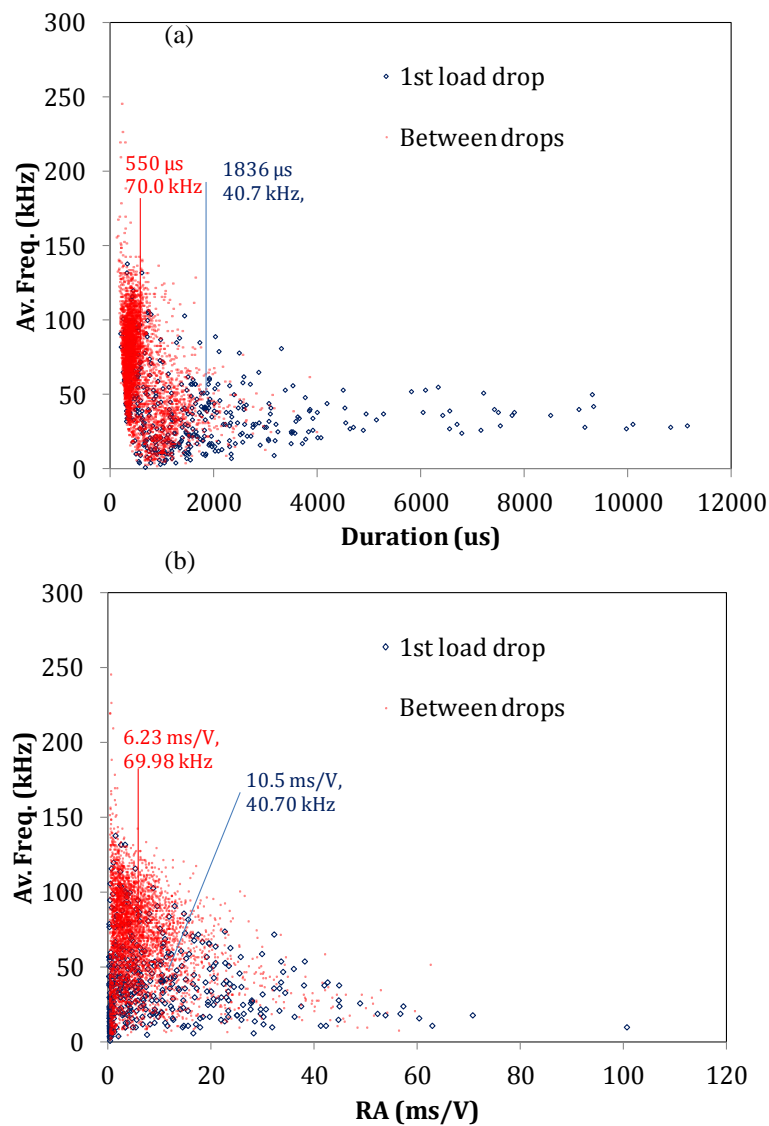

Fig. 7 (a) AF vs. duration and (b) AF vs. RA for all hits captured by broadband sensors

Table 1 Average values of AE features characteristics for different fracture processes

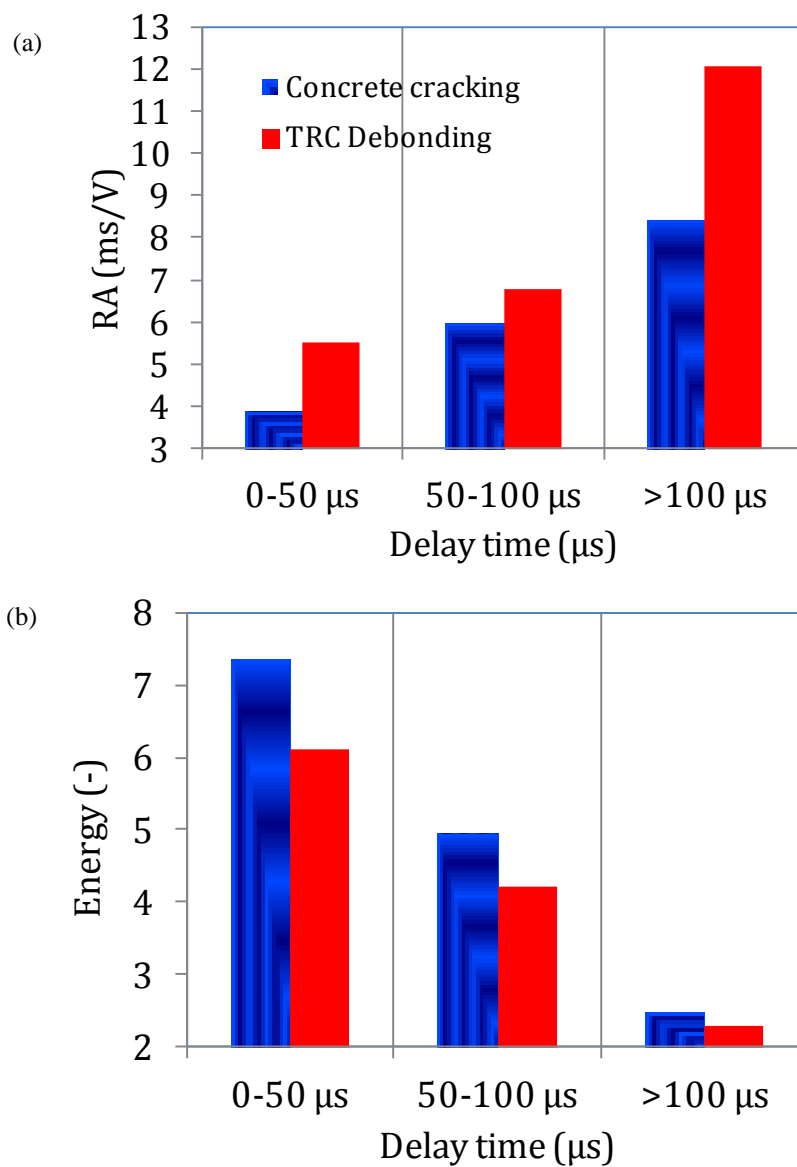|	DUR (µs)	RT (µs)	AF (kHz)	CF (kHz)	RA (ms/V)
Concrete cracking	551	103	70.0	90.8	6.23
TRC Debonding	1836	154.0	40.7	51.7	10.46

Fig. 8 (a) AE Energy and (b) RA vs. the propagation time of the wave

However, due to damping and scattering the energy is reduced, and any concrete cracking signal that propagated a few mm more may carry less energy to the sensor than a debonding one that was recorded close to its origin. It should be stressed out however, that although energy related parameters show a difference between concrete cracking and debonding, this correlation should not be taken for granted. This is due to the fact that the same type of events (e.g., cracking) include creation of small (micro-) or larger (macro-crack) new free surfaces. Accordingly, a debonding event may concern a smaller or larger debonded area. Therefore, the released energy may vary significantly and cannot be considered as robust indicator of the fracture mode. On the other hand, parameters like the rise time or RA value that depend on the wave modes emitted by the transient displacement of the crack sides seem to be more indicative of the fracture mode of the source. Furthermore RA and AF have also been used to characterize the debonding of CFRP strips from concrete (Aggelis *et al*. 2013).
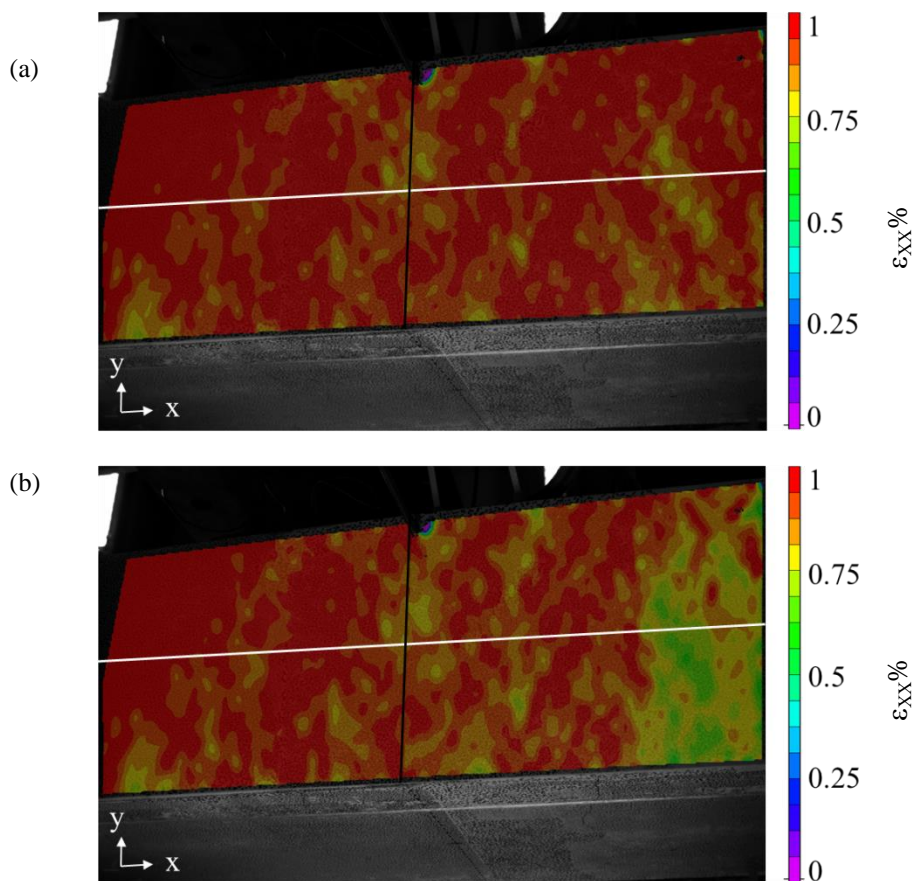

Fig. 9 Strain field parallel to the longitudinal axis (ε_{xx}) as captured (a) before and (b) after the 1st load drop. The vertical black line is the center of the beam

5. Confirmation by DIC

As the external reinforcing layer debonds from the bottom concrete surface its strain is locally decreased. Though debonding is normal to occur at the moments of load drop, DIC confirms this assumption. Fig. 9 shows the longitudinal strain ε_{xx} across the length of the beam before and after the 1st load drop in the TRC reinforced beam (see left arrow in Fig. 5). Locally the strain in the monitored area is strongly reduced. More specifically, strain release is exhibited at the right side for the first load drop (Fig. 9). This is also shown in Fig. 10, where the quantitative strain evolutions in the longitudinal direction of the beam are plotted. The strain distribution is measured at the level of the white lines (center of the beam's width) along the beams axis, as represented in Fig. 9. It is shown that strain in certain parts at the right side of the monitored length reduced by more than 10% indicating that debonding occured at the moments of load drop.

The corresponding strain fields before and after the 2nd load drop (2nd arrow in Fig. 5) are depicted in Figs. 11(a) and 11(b) respectively. In this case greater strain release is exhibited at the left side of the monitored area. Fig. 12 shows the strain along the white line of Figs. 11(a) and 11(b). In this case the strain seems to decrease for longer part of the monitored area, from approximately the middle to the left edge of the monitored area.

By comparing the strain before and after the load drops at each pixel, conclusions about the debonded area are possible. Subtracting the consecutive longitudinal strain fields, yields information on the debonded area. Counting a debonded point as a point with a strain difference of more than 0.1%, results in a debonded area of 13205 mm² and 26850 mm² for the first and second load drops respectively. The threshold value is chosen low, but higher than the noise level (comparison of two pictures in the unloaded stage yields strain variations between -0.046% and 0.046%). It is mentioned that this area is within the visible zone of DIC, while extension of the debonding to further zones cannot be excluded. The debonded areas are represented in Fig. 13.
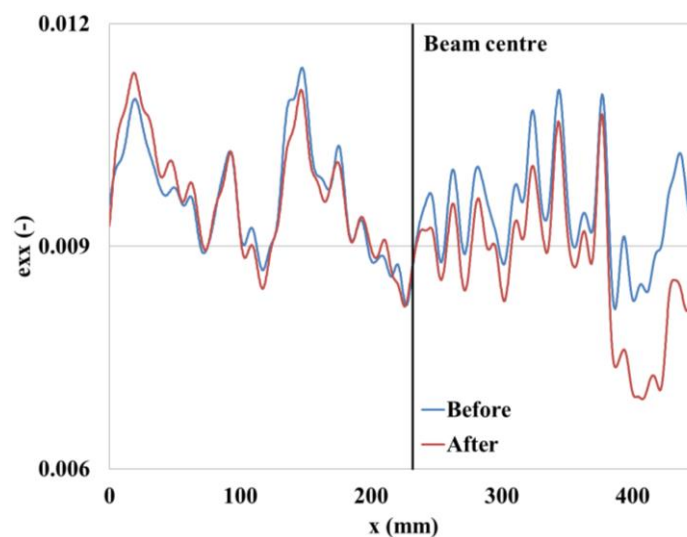

Fig. 10 Strain ε_{xx} parallel to the longitudinal axis of the beam before and after the 1st load drop
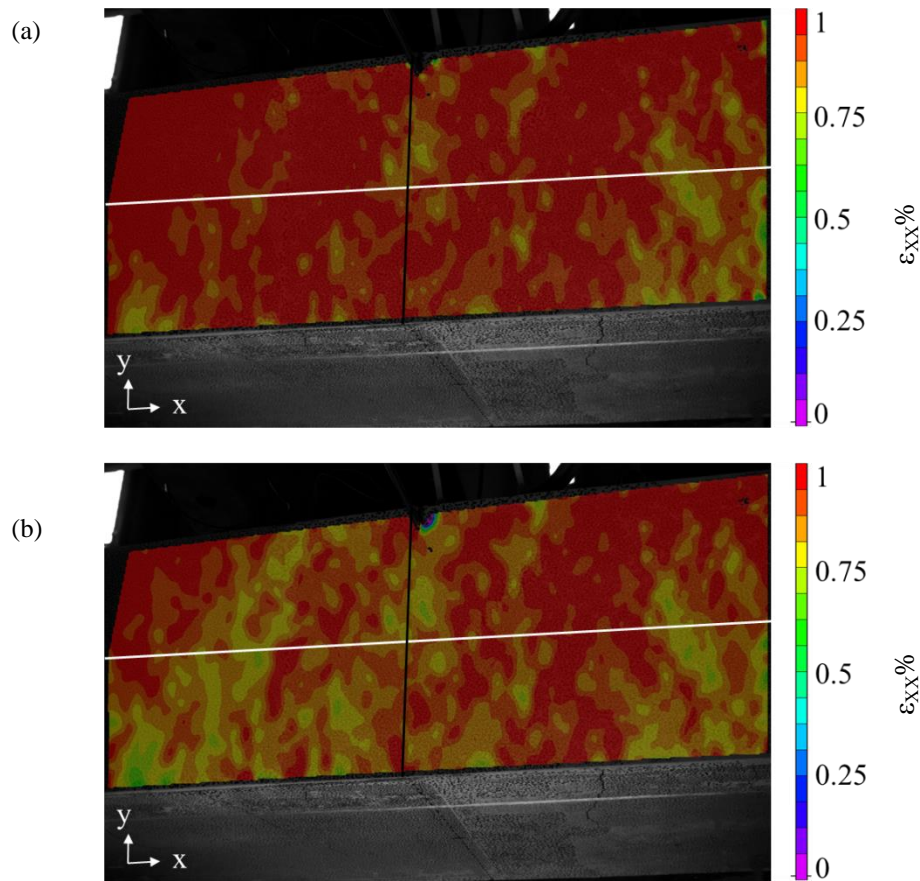
Dimitrios G. Aggelis et al.

Fig. 11 Strain field parallel to the longitudinal axis (ε_{xx}) as captured (a) before and (b) after the 2nd load drop. The vertical black line is the center of the beam
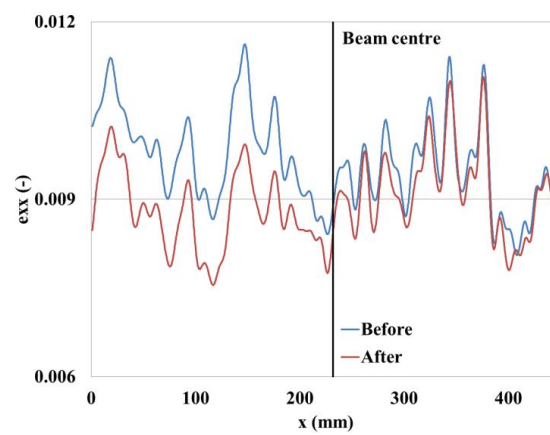

Fig. 12 Strain ε_{xx} parallel to the longitudinal axis of the beam before and after the 2nd load drop
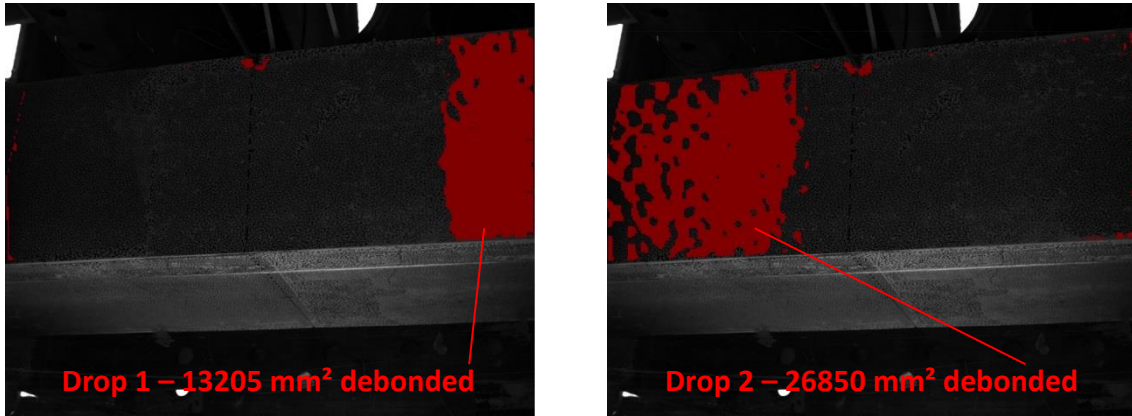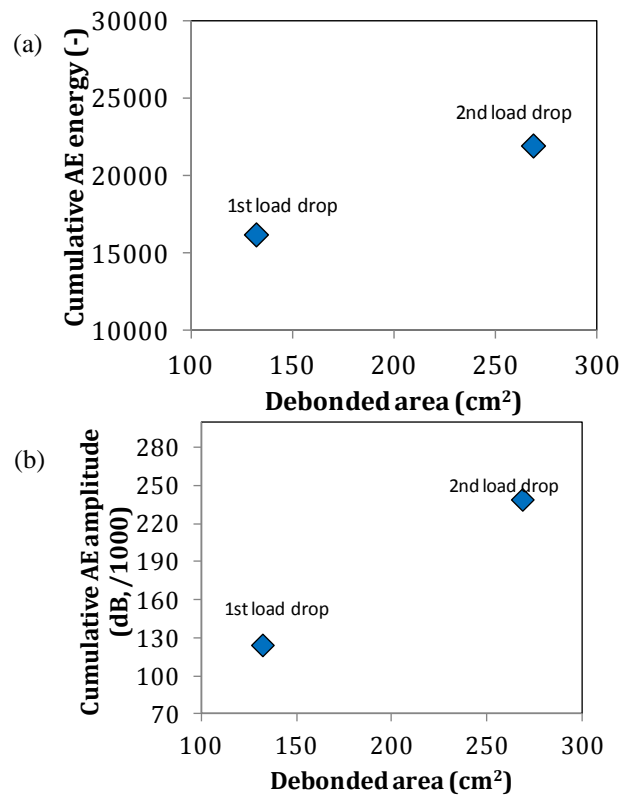
Fig. 13 Debonded areas during both load drops

Fig. 14 (a) Cumulative AE energy and (b) cumulative AE amplitude vs. debonded area of the TRC layer

It is worth mentioning that the quantified extent of debonding during the load drops seems to correlate well with the AE energy parameters received. Isolating the AE activity during the load drop time windows, it was possible to examine the cumulative energy received by all the sensors. It is noticed that the 2nd load drop, escorted by a larger debonded area, as confirmed by DIC, was also escorted by significantly greater amount of AE energy, as seen in the graph of Fig. 14(a)). As another energy-related parameter, the cumulative amplitude of the same number of hits is depicted relatively to the debonded area in Fig. 14(b). The fracture propagation event including the largest area of debonding results in higher intensity of AE. In this form, it would be premature to firmly correlate or try to quantify the debonded area to specific AE values. However, it is shown that except the discrimination between cracking and debonding activity, it is also possible to evaluate the relative severity of different debonding events by AE monitoring. It is mentioned that the existence of debonding was confirmed by the visible separation of the TRC layer from concrete after the experiment, but it could not be possible to assess the exact amount of debonded area better than DIC.

6. Conclusions

The present study concerns mainly AE monitoring of the mechanical behavior of externally reinforced concrete beams under four-point bending. Apart from determination of the onset of cracking for the different forms of reinforcement (TRC and CFRP), the aim was to characterize the fracture mechanisms during loading. It was shown that reinforcement with the high performance TRC layer restrained the cracking, shown by the negligible AE activity at low loads compared to the CFRP strip reinforced and the reference specimen. Additionally, AE trends exhibited sensitivity in the successive loading stages and failure mechanisms. At the moments of temporary load drop, which are verified as debonding of the TRC layer by the release of DIC strain, RA and AE duration values are double or even greater than the corresponding values during stable concrete cracking periods. This AE shift of values shows that AE parameters can be trusted in large size concrete members for the monitoring of the type (mode) of the fracture events. The sensor separation distance is also discussed since strong distortion in AE characteristics can result from the different propagation distance travelled to the various sensors and may compromise the accuracy of characterization. Preliminary correlations between the debonded area and the AE parameters are also reported. Application of DIC simultaneously to AE minimizes the assumptions in the interpretation of the AE as to the actual damage mechanisms since it reveals the changes of the surface strain fields. Examining the behavior of the material system in this simple monotonic loading protocol is a first step towards more complex and possibly dynamic loading schemes that will be more realistic.

References

Aggelis, D.G. (2011), "Classification of cracking mode in concrete by acoustic emission parameters", *Mech. Res. Commun.*, **38**, 153-157.

Aggelis, D.G., Shiotani, T., Papacharalampopoulos, A. and Polyzos, D. (2012), "The influence of propagation path on acoustic emission monitoring of concrete", *Struct. Health Monit.*, **11**(3), 359-366.

Aggelis, D.G., Verbruggen, S., Tsangouri, E., Tysmans, T. and Van Hemelrijck, D. (2013), "Characterization

of mechanical performance of concrete beams with external reinforcement by acoustic emission and digital image correlation", *Constr. Build. Mater.*, **47**, 1037-1045.

Carpinteri, A., Lacidogna, G., Niccolini, G. and Puzzi, S. (2008), "Critical defect size distributions in concrete structures detected by the acoustic emission technique", *Meccanica*, **43**, 349-363.

European Patent Office (2000), "EP 0 861 216 B1, Inorganic resin compositions. Their preparation and use thereof".

Farhidzadeh, A., Dehghan-Niri, E., Salamone, S., Luna, B. and Whittaker, A. (2013), "Monitoring crack propagation in reinforced concrete shear walls by acoustic emission", *J. Struct. Eng. – ASCE*, **139**(12), 04013010. doi:10.1061/(ASCE)ST.1943-541X.0000781

CEB-FIB (2001), fib bulletin 14 Externally bonded FRP reinforcement for RC structures. Lausanne, Switzerland; ISBN 2-88394-054-1.

Ge, M.J. (2003), "The analysis of source location algorithms, Part II: Iterative methods", *J. Acoust. Emission*, **21**, 29-51.

Grosse, C.U. and Ohtsu, M. (2008), *Acoustic emission testing*, Heidelberg, Springer.

Karihaloo, B.L., Ramachandra Murthy, A. and Iyer, N.R. (2013), "Determination of size-independent specific fracture energy of concrete mixes by the tri-linear model", *Cement Concrete Res.*, **49**, 82-88.

Luo, X., Haya, H., Inaba, T. and Shiotani, T. (2006), "Seismic diagnosis of railway substructures by using secondary acoustic emission", *Soil Dynam. Earthq. Eng.*, **26**(12), 1101-1110.

Ohno, K. and Ohtsu, M. (2010), "Crack classification in concrete based on acoustic emission", *Constr. Build. Mater.*, **24**, 2339-2346.

Ohtsu, M. (2010), "Recommendation of RILEM TC 212-ACD: Acoustic emission and related NDE techniques for crack detection and damage evaluation in concrete: Test method for classification of active cracks in concrete structures by acoustic emission", *Mater. Struct.*, **43**(9), 1187-1189.

Ombres L. (2012), "Debonding analysis of reinforced concrete beams strengthened with fibre reinforced cementitious mortar", *Eng. Fract. Mech.*, **81**, 94-109.

Shahidan, S., Pulin, R., Muhamad Bunnori, N. and Holford, K.M. (2013), "Damage classification in reinforced concrete beam by acoustic emission signal analysis", *Constr. Build. Mater.*, **45**, 78-86.

Sutton, M.A., Orteu, J.J. and Schreier, H.W. (2009), *Image Correlation for Shape, Motion and Deformation Measurements. Basic Concepts, Theory and Applications*, Springer Science+Business Media, New York, USA; ISBN 978-0-387-78746-6.

Täljsten, B. and Blanksvärd, T. (2007), "Mineral-based bonding of carbon FRP to strengthen concrete structures", *J. Compos. Constr.*, **11**(2), 120-128.

TRADECC (2007), Technical data sheet: PC® CARBOCOMP.

TRADECC (2009), Technical data sheet: PC® 5800/BL.

Uddin, F.A.K.M., Shigeishi, M. and Ohtsu, M. (2006), "Fracture mechanics of corrosion cracking in concrete by acoustic emission", *Meccanica*, **41**, 425-442.

Van Tittelboom, K., De Belie, N., Lehmann, F. and Grosse, C.U. (2012), "Acoustic emission analysis for the quantification of autonomous crack healing in concrete", *Constr. Build. Mater.*, **28**, 333-341.

Verbruggen, S. (2014), *Reinforcement of concrete beams in bending with externally bonded textile reinforced cementitious composites*, PhD thesis Vrije Universiteit Brussel.

Verbruggen, S., Wastiels, J., Tysmans, T., Remy, O. and Michez, S. (2012), "The influence of externally bonded longitudinal TRC reinforcement on the crack pattern of a concrete beam", *Proceedings of the 3rd international conference on concrete repair, rehabilitation and retrofitting (3-8/9/12)*, Cape Town, South Africa.

Verstrynge, E., Schueremans, L., Van Gemert, D. and Wevers, M. (2009), "Monitoring and predicting masonry's creep failure with the acoustic emission technique", *NDT&E Int.*, **42**(6), 518-523.